

# **Geophysical Research Letters**\*



# RESEARCH LETTER

10.1029/2025GL116351

#### **Key Points:**

- The Tibetan Plateau snow cover (TPSC)-Arctic sea-ice linkage has experienced a regime shift around 1990
- TPSC-driven Arctic circulation anomalies regulate the TPSC-sea-ice connection through modulating polar vortex dynamics
- TPSC phase transitions modulate Arctic sea-ice melt and growth via affecting moisture and solar radiation anomalies

#### **Supporting Information:**

Supporting Information may be found in the online version of this article.

#### Correspondence to:

C. Zhang and A. Duan, chaozhang@xmu.edu.cn; amduan@xmu.edu.cn

#### Citation:

Zhang, C., Duan, A., Jia, X., & Liu, S. (2025). Connecting Tibetan Plateau snow change with Arctic sea-ice. *Geophysical Research Letters*, *52*, e2025GL116351. https://doi.org/10.1029/2025GL116351

Received 7 APR 2025 Accepted 9 JUL 2025

#### **Author Contributions:**

Conceptualization: Chao Zhang Data curation: Shizuo Liu Formal analysis: Chao Zhang, XiaoJing Jia

Funding acquisition: Chao Zhang,

Anmin Duan

Investigation: Chao Zhang, XiaoJing Jia,

Shizuo Liu

Methodology: Chao Zhang Project administration: Anmin Duan Resources: Chao Zhang, Shizuo Liu Software: Chao Zhang

Supervision: Anmin Duan Validation: Chao Zhang Visualization: Chao Zhang Writing – original draft: Chao

Writing – original draft: Chao Zhang Writing – review & editing: Chao Zhang, Anmin Duan, XiaoJing Jia

#### © 2025 The Author(s).

This is an open access article under the terms of the Creative Commons Attribution-NonCommercial License, which permits use, distribution and reproduction in any medium, provided the original work is properly cited and is not used for commercial purposes.

# **Connecting Tibetan Plateau Snow Change With Arctic Sea-Ice**

Chao Zhang<sup>1,2</sup>, Anmin Duan<sup>1</sup>, XiaoJing Jia<sup>3</sup>, and Shizuo Liu<sup>4</sup>

<sup>1</sup>Center for Marine Meteorology and Climate Change, College of Ocean and Earth Sciences, State Key Laboratory of Marine Environmental Science, Xiamen University, Xiamen, China, <sup>2</sup>Marine Biogeochemistry Division, GEOMAR Helmholtz Centre for Ocean Research Kiel, Kiel, Germany, <sup>3</sup>Key Laboratory of Geoscience Big Data and Deep Resource of Zhejiang Province, School of Earth Sciences, Zhejiang University, Hangzhou, China, <sup>4</sup>Nicholas School of the Environment, Duke University, Durham, NC, USA

**Abstract** Documenting changes in the Arctic sea-ice variability are essential for understanding the spring sea-ice predictability barrier. While Tibetan Plateau snow cover (TPSC) has been linked to Arctic sea-ice variability, the spatiotemporal stability of this relationship remains unclear. In this study, combing satellite observations and snow experiments, we identified a shift in connections between TPSC and Barents-Kara Seas sea-ice around 1990. Before 1990, a positive dipole TPSC pattern (eastern enhanced/western reduced snow cover) induces Arctic anticyclonic anomalies through a circumglobal wave train. These anomalies facilitate polar vortex splitting, enhancing moisture transport and solar radiation over the northern Kara Sea, which accelerates sea-ice reduction. Conversely, post-1990, a positive monopole TPSC pattern (positive snow anomalies on the entire Tibetan Plateau) strengthens the polar vortex, suppressing Barents Sea (BS) moisture and solar radiation, thereby promoting sea-ice growth. This regime shifts underscore TPSC's capacity to modulate Arctic sea-ice dynamics through polar vortex system.

Plain Language Summary Investigating the causes and driving mechanisms behind year-to-year variations in Arctic sea-ice is important for understanding its spring prediction barrier. This study reveals how shifting snow patterns on the Tibetan Plateau (TP), Earth's Third Pole, drive Arctic sea-ice fluctuations. Before 1990, positive phase of out-phase TP snow distribution (heavier snow in the Plateau's east and lighter snow in the west) favors Arctic anticyclonic circulation anomalies (wind pattern). Such wind distribution weakens the polar vortex, a key circulation system, and promoting warm, moist air into the northern Kara Sea. This combination melts sea-ice rapidly. After 1990, positive phase of TP snow cover (unform snow gains across the Tibetan) strengthens the polar vortex, blocking warm and air inflow to the Barents Sea and allowing ice growth. These findings show how Tibetan snow changes "steer" Arctic sea-ice conditions through atmospheric waves and energy shifts, offering mechanistic insights to seasonal sea-ice predictability.

# 1. Introduction

Arctic sea-ice, a critical climate change indicator, has exhibited a dramatic decline in recent decades (England et al., 2020; Simmonds & Li, 2021; Thackeray & Hall, 2019), with variability spanning synoptic (Cohen et al., 2021), interannual (Deng & Dai, 2024; Luo et al., 2023), and interdecadal scales (Day et al., 2012; Deng & Dai, 2022; Ding et al., 2019; Zhou et al., 2024). Approximately 8,000 km³ of sea-ice volume loss has occurred since 1979 (Schweiger et al., 2011), driven by persistent anthropogenic forcing (Dai et al., 2019; England et al., 2020) and natural variability linked to Arctic atmospheric circulation anomalies (Ding et al., 2017). Winter sea-ice interannual variability primarily centers on the Barents-Kara Seas (BKS, Kim et al., 2014; Luo et al., 2023). This BKS (He et al., 2023; Luo et al., 2023), its subsequent El Niño-Southern Oscillation (ENSO) influence (Chen et al., 2020, 2024), and ENSO modulation mechanisms (Xie et al., 2025) exhibit marked decadal changes.

Arctic sea-ice variabilities across interannual and longer timescales arises from atmospheric and oceanic processes spanning tropical (Clancy et al., 2021; Topál et al., 2022) and mid-to-high latitudes (Stone et al., 2020; Sumata et al., 2023; P. Zhang et al., 2023). Tropical drivers such as the ENSO modulate interannual variability of Arctic sea-ice through atmospheric teleconnections via the Pacific-North-American and Atlantic pathways (Liu et al., 2021; Luo et al., 2023). Mid-to-high latitude systems, including the Asian-Pacific Oscillation (Zhou et al., 2024), Atlantic meridional overturning circulation (Johns et al., 2011; Mahajan et al., 2011), and North

ZHANG ET AL. 1 of 12

Atlantic Oscillation (NAO) (Ding et al., 2014; Luo et al., 2017, 2019), govern sea-ice variability in summer, autumn, and winter. However, the mechanisms controlling spring sea-ice remain poorly understood, despite the challenges posed by the "spring predictability barrier" for Arctic sea-ice (Bushuk et al., 2020; C. Zhang, Duan, Jia, Wang, & Pan, 2023), highlighting the urgency to identify interannual drivers during this transitional season.

The Tibetan Plateau (TP), Earth's highest and most extensive highland system, functions as a pivotal "Asian Water Tower" sustaining regional hydrological cycles (Immerzeel et al., 2020; Xu et al., 2008, 2021). Tibetan Plateau snow cover (TPSC) serves as a moisture source for downstream areas (Kraaijenbrink et al., 2021; Smith & Bookhagen, 2018) and exhibits hemispheric-scale climatic influence extending to polar regions (Xu et al., 2021). Emerging research highlights TPSC's role in Arctic climate dynamics (Tang et al., 2024; C. Zhang, Duan, Jia, Wang, & Pan, 2023). For instance, C. Zhang, Duan, Jia, Wang, & Pan (2023) has linked increased TPSC to reduced Arctic sea-ice via cyclonic circulation and equatorward ice transport, while S. Liu, et al. (2022) identified TPSC-driven anticyclonic patterns that accelerate ice melt. These discrepancies underscore unresolved debates regarding TPSC-Arctic linkages and their governing pathways.

Both TPSC (C. Zhang et al., 2022; C. Zhang, Jia, et al., 2023) and Arctic sea-ice (He et al., 2023; Luo et al., 2023) have undergone marked interannual regime shifts since the early 1990s. Observational evidence shows a dynamical transition in spring TPSC-sea-ice linkages (Figure S1 in Supporting Information S1). With TPSC evolving from dipole-dominated to monopole-driven patterns, linkage between TPSC and northern Kara Sea (NKS) sea-ice variability reduce, whereas persistent significant Barents Sea (BS) sea-ice observed. To examine these shifts, this study employs a multi-method framework integrating observational diagnostics, snow-forcing experiments using the Community Earth System Model Large Ensemble (CESM-LE), and information flow causality analysis, offering novel mechanistic insights into the changes in the TP-Arctic climate linkages. In the following, Section 2 details the data sources, methodological framework, and model experiments. Section 3 analyzes the main results. Section 4 provides the conclusions and discussions.

#### 2. Data and Methods

# 2.1. Data

We use historical records from 1970 to 2020: (a) The satellite-derived weekly snow cover extent (SCE) data sets have a 25 km resolution in the National Snow and Ice Data Center (NSIDC) (Brodzik & Armstrong, 2013) and 89 × 89 cell grids in the National Oceanic and Atmospheric Administration (NOAA) Climate Data Record (Robinson et al., 2012), respectively. (b) Monthly mean 1° resolution sea ice concentration data are available at the Hadley Center Sea Ice and Sea Surface Temperature data set (HadISST) (Rayner et al., 2003). (c) Daily Polar Pathfinder sea-ice motion vectors with a 25 km resolution are provided by the NSIDC (Tschudi et al., 2019). (d) Monthly mean 0.25° resolution surface wind stress are derived from the fifth generation of ECMWF's ocean reanalysis system and its real-time analysis component (ORAS5) (Zuo et al., 2018). (e) Atmospheric variables are obtained by the ERA5 (Hersbach et al., 2020). (f) Monthly mean 2.5° resolution precipitation are derived from the Global Precipitation Climatology Project (GPCP) (Adler et al., 2003).

#### 2.2. Methods

The information flow, as deduced from the first principle, can be used to evaluate quantitative causation (Liang & Kleeman, 2005), which has been widely applied in various fields, including climate change attribution, Arctic sea-ice anomalies, quantum information, and drought detection (Goodwell et al., 2020; Yi & Bose, 2022; C. Zhang, Duan, Jia, Wang, & Pan, 2023). To determine the TPSC-sea ice causation, we calculate their information flow based on the following equations (Liang, 2016; Liang & Kleeman, 2005).

$$C_{ij} = \overline{(x_i - \overline{x_i})(x_i - \overline{x_i})} \tag{1}$$

$$\dot{x}_{i,n} = (x_{i,n+k} - x_{i,n})/k\Delta t \tag{2}$$

$$\hat{T}_{2\to 1} = \frac{C_{11}C_{12}C_{2,d1} - C_{12}^2C_{1,d1}}{C_{11}^2C_{22} - C_{11}C_{12}^2} \tag{3}$$

ZHANG ET AL. 2 of 12

where  $C_{i,j}$  refers to the covariance between series  $x_i$  and series  $x_j$ .  $\Delta t$  represents the time step.  $C_{i,dj}$  is determined as the sample covariance between  $x_i$  and the Euler forward difference scheme in Equation 2.  $\hat{T}_{2\rightarrow 1}$  represents the information flow from variable  $x_2$  to variable  $x_1$ . Based on the information theory,  $\hat{T}_{2\rightarrow 1} \neq 0$  denotes that the  $x_2$  has a causal impact on  $x_1$ ; whereas  $\hat{T}_{2\rightarrow 1} = 0$  means no causal influence.

In this study, significant differences in polar vortex system sweep over the Atlantic-European sectors. Therefore, the polar vortex areas is calculated using the following equation:

$$PVA = \int_{\varphi}^{\frac{\pi}{2}} \int_{\lambda_1}^{\lambda_2} R^2 \cos \varphi \, d\varphi \, d\lambda = R^2 (1 - \sin \varphi)(\lambda_2 - \lambda_1)$$
 (4)

where R refers to the radius of the earth. The variable  $\varphi$  represents the latitude of the southern boundary of the polar vortex, determined by the eigen-contour lines of 500 hPa geopotential height (552 dagpm in March and April, 560 dagpm in May). The variable  $\lambda$  is longitude, spanning from 30°W to 60°E over the Atlantic-European sectors

Additional diagnostic methodologies, encompassing moisture source-sink analysis and atmospheric wave dynamics diagnostics, are detailed in Supporting Information S1.

# 2.3. Realistic TPSC Experiments Using CESM-LE

Numerical experiments targeting snowpack dynamics have proven particularly challenging over the TP, primarily due to complex high-altitude interactions. Notably, simulated TPSC trend frequently contradicts observational records (Gottlieb & Mankin, 2024). Model results frequently fail to capture key region affected by snow cover (Preece et al., 2023; T. Zhang et al., 2019). Although the snow-hydrological feedback mechanism significantly influences atmospheric circulation patterns (Xiao & Duan, 2016; Yasunari et al., 1991; C. Zhang & Jia, 2022), many previous studies have substituted high albedo or diabatic cooling for snow forcing (Wang et al., 2017; C. Zhang & Jia, 2022). To address this limitation, we employ a novel snow physics framework within the NCAR Community Earth System Model (CESM1.(b) Large Ensemble (CESM-LE) (Kay et al., 2015), resolving both snow-albedo and snow-hydrological effects.

We design realistic snow experiment using CESM-LE's 60-member ensemble to investigate hemispheric-scale teleconnections and Arctic climate anomalies induced by TPSC anomalies. The CESM-LE integrates the components including: the Community Atmosphere Model (CAM4) (Neale et al., 2013), the Community Land Model (CLM4.5) (Oleson et al., 2013), and other components, all coupled at a resolution of  $2.5^{\circ} \times 1.875^{\circ}$  (longitude × Latitude).

Four snow perturbation experiments are conducted using observational TPSC anomaly fields (Table S1 in Supporting Information S1). Given the high consistency between NOAA and NSIDC snow data sets in capturing TPSC spatial patterns (Figure S2 in Supporting Information S1), we select NOAA snow data to force the CESM-LE. For the pre-1990 period (1970–1989), we design two experiments initialized with spring climatological atmospheric and oceanic conditions. The TPSC anomaly fields are added as the forcing fields. Specifically, we conduct a positive dipole-like TPSC experiment (Pos<sup>Dp</sup><sub>exp</sub>), by using positive phase of leading Empirical orthogonal function (EOF) mode of spring TPSC pattern during 1970–1989 as the force fields. Similarly, we perform a counterpart negative dipole experiment (Neg<sup>Dp</sup><sub>exp</sub>) using negative phase of leading EOF mode of spring TPSC pattern during this period. In model simulation, each 60-member is run from March 1 to May 31 during 1970–1989, with observed TPSC anomalies replacing climatological snow fields over the TP to drive CESM-LE. The model responses to dipole-like TPSC experiments are evaluated as the ensemble mean difference between Pos<sup>Dp</sup><sub>exp</sub> and Neg<sup>Dp</sup><sub>exp</sub>, reflecting the responses to dipole TPSC forcing.

The setups for the latter two experiments are similar to the first two but for the conditions during 1991–2020. The positive and negative monopole TPSC experiments ( $Pos_{exp}^{Mp}$  and  $Neg_{exp}^{Mp}$ ) are conducted using the positive and negative phases of the leading TPSC mode after 1990, respectively. All simulations employ 60-member ensemble and each member's integration period spans from March 1 to May 31 during 1991–2020, during which the monopole TPSC anomaly fields replace the original snow field to drive the CESM-LE. The other setups follow

ZHANG ET AL. 3 of 12

the initialization and forcing protocols in the first two experiment. We evaluate the model responses to monopole TPSC forcing by analyzing the ensemble mean difference between  $Pos_{exp}^{Mp}$  and  $Neg_{exp}^{Mp}$ .

Numerical experiments with 60 simulation members successfully reproduce the transition in the TPSC patterns (Figure S3 in Supporting Information S1). Over 85% of the members exhibit reliable snow simulation performance, and all members reproduce the changes in the TPSC patterns (Figures S3e and S3j in Supporting Information S1). Consequently, the ensemble mean difference from all 60 simulations is utilized to represent the model's responses to TPSC forcing in the subsequent analysis.

#### 2.4. Statistical Analysis

A Gaussian filter is employed to extract the interannual variability of all variables by applying an 8-year high-pass filter. Statistical significance is assessed using a two-tailed Students's *t* test.

#### 3. Results

#### 3.1. Changes in the TPSC-Sea-Ice Linkage

On the interannual timescale, snow cover variations between the eastern and western TP exhibits a significant negative correlation prior to 1990, which shifts to a significant positive correlation after 1990 (Figure S4 in Supporting Information S1). This shift reflects a pre-1990 dipole TPSC pattern, contrasting with post-1990 monopole variability, aligning with our previous reported interdecadal transition in TPSC structures (C. Zhang, Jia, et al., 2023; C. Zhang et al., 2022).

Empirical orthogonal function analysis further reveals this interannual-scale transition in TPSC, with different snow cover data sets consistently capturing the pre-1990 dipole structure and post-1990 monopole variation (Figure S2 in Supporting Information S1). To examine potential linkages with Arctic sea-ice anomalies, we analyze the time series of the first principal component of TPSC (PC1\_TPSC), focusing on the NKS and BS regions where TPSC-associated sea-ice anomalies are most prominent (Figure S1 in Supporting Information S1).

Sliding correlation analysis reveals a distinct temporal evolution in the TPSC-sea-ice relationship (Figure 1a). Prior to 1990, PC1\_TPSC and NKS sea-ice display a robust negative correlation (r=-0.53, p<0.05), which diminishes post-1990 (r=-0.02, p>0.1). Concurrently, PC1\_TPSC and BS sea-ice transform from a statistically insignificant positive correlation before 1990 (r=0.30, p>0.1) to a significant positive correlation post-1990 (r=0.51, p<0.05; Figure 1a). These results indicate that the positive phase of dipole TPSC pattern corresponds to reduced NKS sea-ice anomalies before 1990, while the positive phase of monopole TPSC structure coincides with enhanced BS sea-ice anomalies after 1990, marking a shift in the interannual relationship between TPSC and Arctic sea-ice around 1990.

To further validate this transition, we divide the analysis into pre-1990 (1970–1989) and post-1990 (1991–2020) periods. The earlier dipole TPSC phase shows a significant negative correlation with NKS sea-ice (r = -0.67, p < 0.01; Figures 1b and 1c). Conversely, the latter dipole TPSC period exhibits a significant positive correlation with BKS sea-ice (r = 0.59, p < 0.01; Figures 1d and 1e). This opposite correlation signs between two periods confirm a reversal in TPSC-sea ice linkages around 1990.

Notably, since contemporaneous regressions cannot resolve causal directionality, we employ information flow theory to rigorous assess causal relationships between TPSC and Arctic sea-ice anomalies. This framework quantifies causal relationships by evaluating how one system state (e.g., TPSC) predicts state of another variable (e.g., sea-ice), where flow direction identifies causality and magnitude reflects its strength (Liang & Kleeman, 2005; Liang, 2016; see Methods). Critically, dominant information flow pathways shift over time: pre-1990, causal influence originates from PC1\_TPSC toward NKS sea-ice anomalies, whereas post-1990, causality is from PC1\_TPSC to BS sea-ice anomalies (Figures 1f and 1g). This spatiotemporal pattern, along with TPSC consistently acting as the causal driver and effected regions transitioning from NKS to BS, provides robust evidence that TPSC has causal influence on NKS/BS sea-ice variability.

ZHANG ET AL. 4 of 12

19448007, 2025, 14, Downloaded from https://agupubs.onlinelibrary. wiley.com/doi/10.1029/2025GL116351 by Chao Zhang - Xiamen University, Wiley Online Library on [16.07/2025]. See the Terms

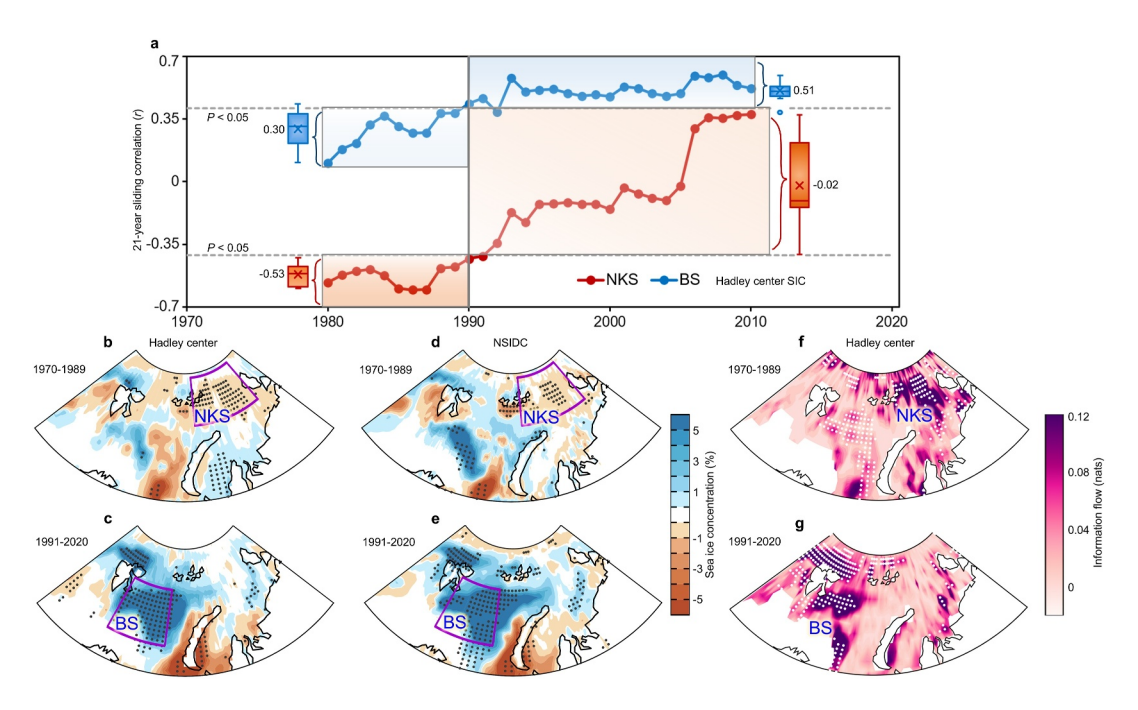


Figure 1. Changes in the snow-ice relationship. (a) The 21-year sliding temporal correlation between spring PC1\_TPSC and sea-ice concentration (Hadley Center data set) over the northern Kara Sea (NKS) and Barents Sea (BS) during 1970–2020. Box charts show the corresponding correlations before and after 1990. (b, c) Spring sea-ice concentration anomalies obtained by regression onto PC1\_TPSC for (b) 1970–1989 and (c) 1991–2020 using Hadley Center data. (d, e) Same as in (b, c) but for National Snow and Ice Data Center sea-ice concentration data. The purple boxes indicate the NKS ( $58^{\circ}E-93^{\circ}E$ ,  $78^{\circ}N-83^{\circ}N$ ) and BS ( $23^{\circ}E-45^{\circ}E$ ,  $73^{\circ}N-79^{\circ}N$ ). (f, g) Information flow from PC1\_TPSC to spring sea-ice concentration for (f) 1970–1989 and (g) 1991–2020, based on Equations 1–3. Stippling indicates areas with significant sea-ice anomalies at the 95% confidence level (p < 0.05). All variables are expressed as interannual anomalies.

#### 3.2. Influence of Atmospheric Teleconnections on Arctic Circulation Changes

Significant alternations in local albedo feedback, hydrological effects, and vorticity source perturbations are driven by shifts in TPSC patterns (Figures S5 and S6 in Supporting Information S1; see text in Supporting Information S1). Notably, TPSC as a driver of atmospheric wave trains through diabatic cooling and anomalous perturbations (Li et al., 2018; Liu et al., 2022; Xiao & Duan, 2016; C. Zhang, Duan, Jia, Hu, & Liu, 2023; C. Zhang et al., 2021). We therefore investigate whether these localized changes trigger teleconnections with Arctic circulation through observation analysis, CESM-LE snow experiments, and information flow causality analysis.

Prior to 1990, the dipole TPSC pattern associate with mid-to-high latitude wave flux propagation across the Northern Hemisphere (Figure S7a in Supporting Information S1). These fluxes are accompanied by alternating positive and negative height anomaly centers (Figure 2a), and similar temperature anomaly centers (Figure S8a in Supporting Information S1). Critically, these patterns of atmospheric anomaly centers are captured in both snow simulation experiments (Figure 2c and Figure S8c in Supporting Information S1) and the information flow causality maps (Figure 2e and Figure S8e in Supporting Information S1), demonstrating that dipole TPSC structure exert causal influence on the circumglobal wave train.

Post-1990, however, the transition to a monopole TPSC variation corresponds to an extended wave flux pathway (Figure S7b in Supporting Information S1). This longer route accompanies additional centers of height anomaly centers (labeled 1 to 10, Figure 2b) and thermal anomaly centers (Figure S8b in Supporting Information S1) in observations. Crucially, both model simulations (Figure 2d and Figure S8d in Supporting Information S1), and information flow (Figure 2f and Figure S8f in Supporting Information S1) diagnostics capture those atmospheric anomaly centers, confirming the monopole TPSC's causal role in amplifying hemispheric-scale atmospheric waviness.

Notably, beyond altered pathways of atmospheric wave propagations, the Arctic exhibits a reversal in circulation anomalies associated with TPSC-driven wave trains. Before 1990, the upper troposphere over the Arctic is

ZHANG ET AL. 5 of 12

19448007, 2025, 14, Downloaded from https://agupubs.onlinelibrary. wiley.com/doi/10.1029/2025GL116351 by Chao Zhang - Xiamen University, Wiley Online Library on [16.07/2025]. See the Terms

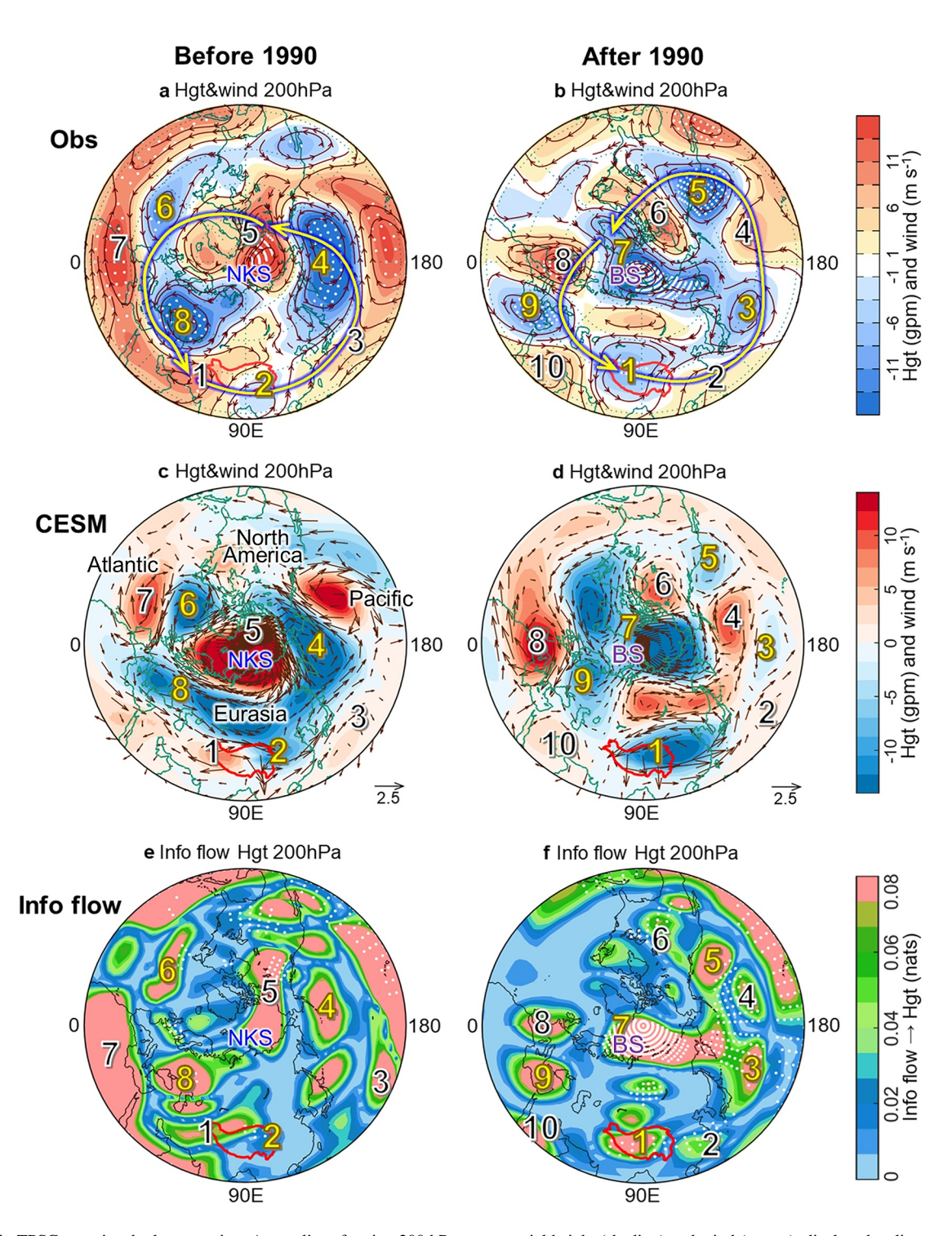
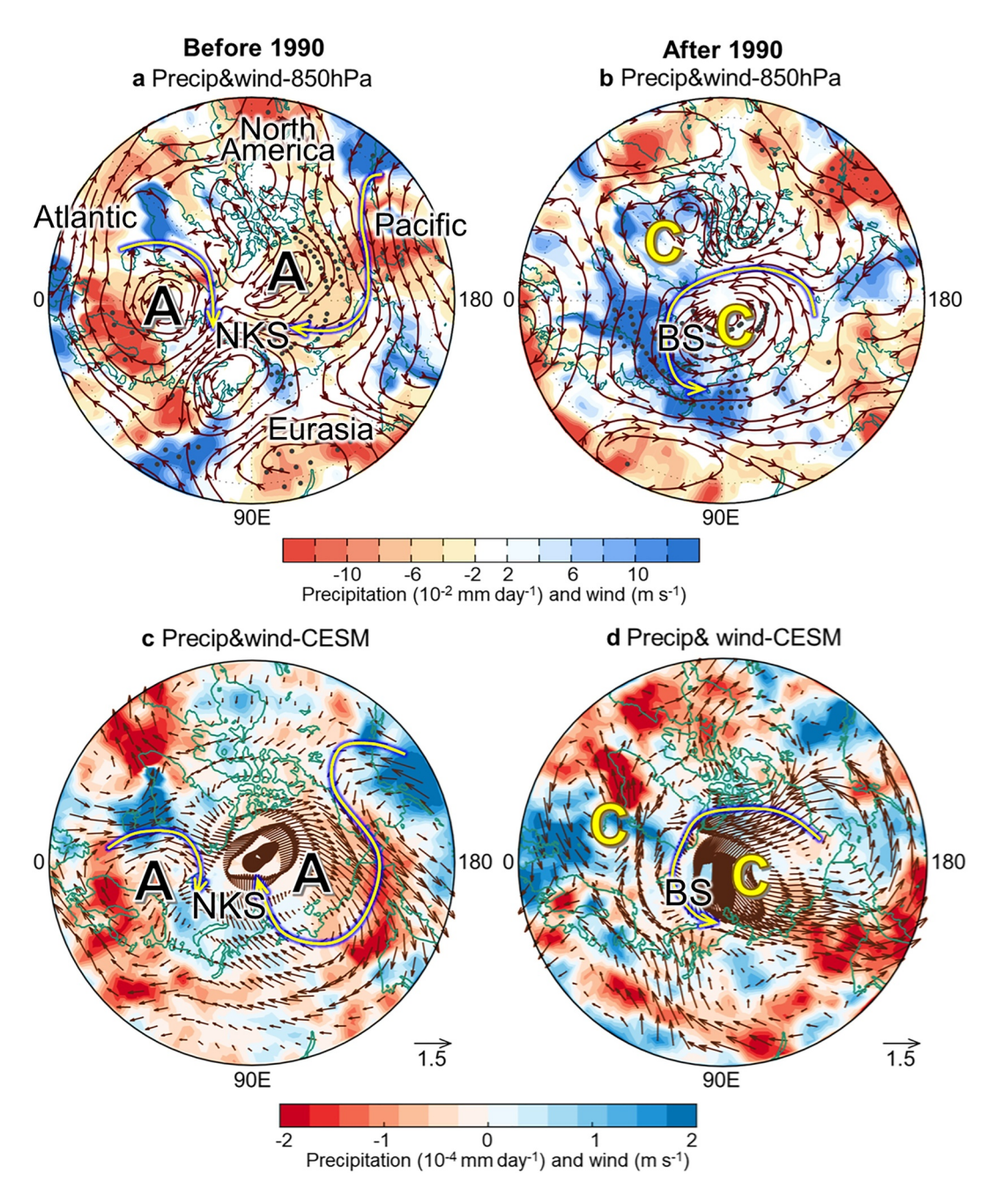


Figure 2. Shift in TPSC-associated teleconnection. Anomalies of spring 200 hPa geopotential height (shading) and wind (vector), displayed as linear regression with respect to PC1\_TPSC for (a) before and (b) after 1990. Thick yellow arrows denote the schematic propagation of the atmospheric wave trains (see Figure S7 in Supporting Information S1 for details). (c, d) As in (a, b), but representing dipole and monopole Tibetan Plateau snow cover experiments using Community Earth System Model Large Ensemble, shown as the ensemble mean difference: (c) before 1990 (Pos<sup>bp</sup><sub>exp</sub>-Neg<sup>bp</sup><sub>exp</sub>) and (d) after 1990 (Pos<sup>kp</sup><sub>exp</sub>-Neg<sup>kp</sup><sub>exp</sub>). (e, f) As in (a, d), but showing causal information flow from PC1\_TPSC to the geopotential height fields. Dots mark areas with statistical significance at the 95% confidence level. Yellow and black numbered symbols represent negative and positive height anomalies, respectively. All data sets reflect interannual variability.

ZHANG ET AL. 6 of 12

19448007, 2025, 14, Downloaded from https://agupubs.onlinelibrary. wiley.com/doi/10.1029/2025GL116351 by Chao Zhang - Xiamen University, Wiley Online Library on [16.07/2025]. See the Terms



**Figure 3.** Arctic precipitation and circulation responses to different Tibetan Plateau snow cover (TPSC) forcings. Spring precipitation (shading) and 850 hPa wind (vectors) anomalies, displayed as linear regression with respect to PC1\_TPSC for (a) before and (b) after 1990. (c, d) As in (a, b), but for dipole and monopole TPSC forcing experiments, shown as the ensemble mean difference: (c) before 1990 (Pos<sup>Dp</sup><sub>exp</sub>–Neg<sup>Dp</sup><sub>exp</sub>) and (d) after 1990 (Pos<sup>Mp</sup><sub>exp</sub>–Neg<sup>Mp</sup><sub>exp</sub>). Black dots indicate areas with statistical significance at the 95% confidence level. Letter of "A" and "C" denotes the anticyclonic and cyclonic circulation anomalies, respectively. The thick yellow arrows denote the direction of airflow. All data exclusively captures interannual-scale variability.

dominated by anticyclonic anomalies (Figure 2a), which transition to cyclonic anomalies post-1990 (Figure 2b). This vertical structure persists into the lower troposphere (Figure 3), forming a barotropic circulation structure in the Arctic. Furthermore, these circulation regimes couple with opposing thermal anomalies, with warming anomalies before 1990 (Figures S8a in Supporting Information S1) versus cooling anomalies after 1990 (Figure S8b in Supporting Information S1), that directly modulate Arctic sea-ice variability. Collectively, TPSC-

ZHANG ET AL. 7 of 12

19448007, 2025, 14, Downloaded from https://agupubs.onlinelibrary.wiky.com/doi/10.1029/2025GL116351 by Chao Zhang - Xiamen University , Wiley Online Library on [16.07/2025]. See the Terms and Conditions (https://agupubs.onlinelibrary.wiky.com/doi/10.1029/2025GL116351 by Chao Zhang - Xiamen University , Wiley Online Library on [16.07/2025]. See the Terms and Conditions (https://agupubs.onlinelibrary.wiky.com/doi/10.1029/2025GL116351 by Chao Zhang - Xiamen University , Wiley Online Library on [16.07/2025]. See the Terms and Conditions (https://agupubs.onlinelibrary.wiky.com/doi/10.1029/2025GL116351 by Chao Zhang - Xiamen University , Wiley Online Library on [16.07/2025]. See the Terms and Conditions (https://agupubs.com/doi/10.1029/2025GL116351 by Chao Zhang - Xiamen University , Wiley Online Library on [16.07/2025]. See the Terms and Conditions (https://agupubs.com/doi/10.1029/2025GL116351 by Chao Zhang - Xiamen University , Wiley Online Library on [16.07/2025].

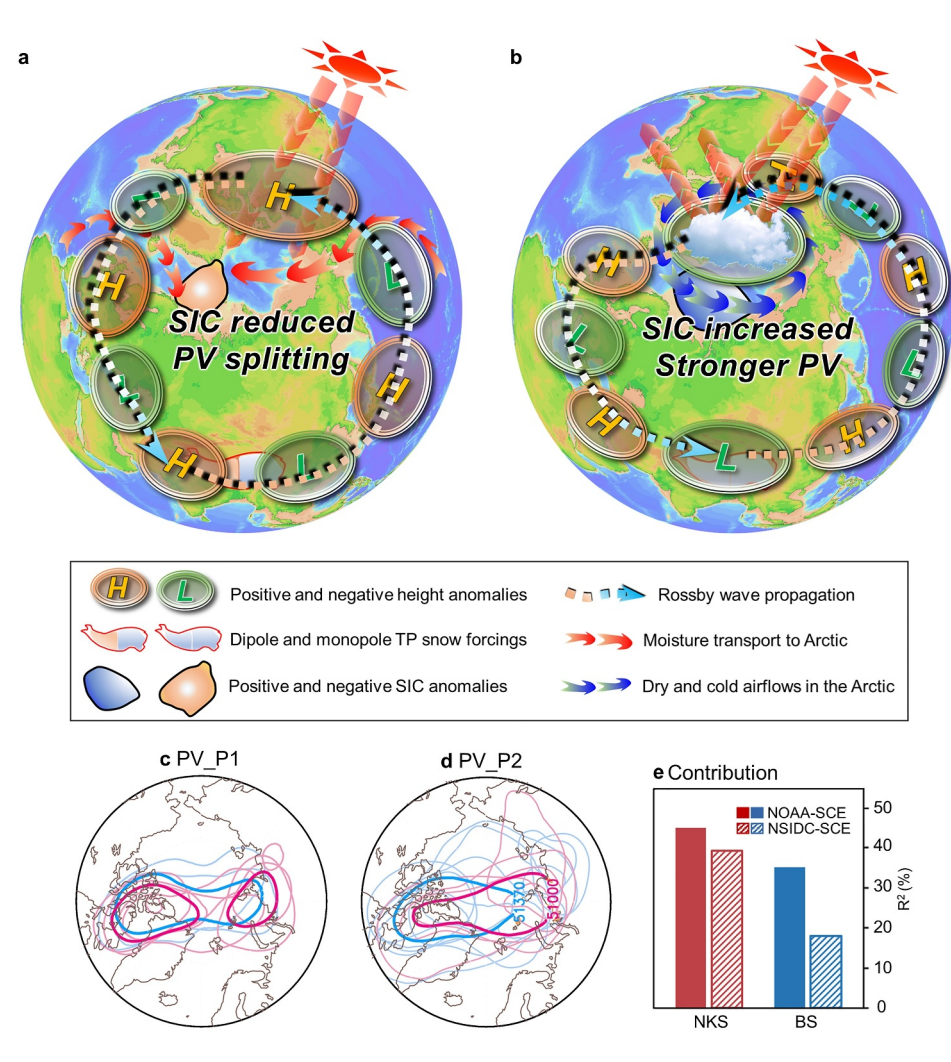


**Figure 4.** Schematic diagrams illustrate the impact of the positive phase of dipole and monopole Tibetan Plateau snow cover (TPSC) patterns on the Arctic sea-ice variability (a) before and (b) after 1990, respectively. The composite of spring Arctic polar vortex for extreme positive (thick red line) and negative (thick blue line) PC1\_TPSC years (c) before and (d) after 1990. The thin lines show the Arctic polar vortex during each extreme TPSC years (see Table S2 in Supporting Information S1 for details). The Arctic polar vortex is represented by the  $51,000 \text{ m}^2 \text{ s}^{-2}$  geopotential height at 500 hPa, with the  $51,370 \text{ m}^2 \text{ s}^{-2}$  line in (d) for comparison. (e) The contribution of National Oceanic and Atmospheric Administration (solid bars) and National Snow and Ice Data Center (slash bars) TPSC impacts on the sea-ice interannual variability over the northern Kara Sea for 1970-1989, and the BS for 1991-2020.

associated circumglobal wave trains act as a dynamic atmospheric bridge, teleconnecting TPSC to phase-reversed Arctic circulation patterns, thereby generating distinct signatures on Arctic climate variability.

# 3.3. Mechanisms of Reversed Impact of TPSC on Arctic Sea-Ice

To gain insight into the mechanisms, we analyze how TPSC modulates thermal and dynamic processes governing sea-ice variability. Within atmospheric circulation systems, the Arctic polar vortex emerges as a critical mediator linking mid-to-high latitude climate systems to Arctic anomalies (Cohen et al., 2021; Kim et al., 2014).

Prior to 1990, positive dipole TPSC-associated anticyclonic anomalies weaken the climatological Arctic polar vortex, leading to its separation into dual centers (red circles in Figure 4c). The correlations between the polar vortex location index and PC1\_TPSC are r = -0.47 (p < 0.05) before 1990 and r = 0.23 (p > 0.1) after 1990 (Figure S9a in Supporting Information S1), indicating dipole TPSC pattern dominance in impacting polar vortex location before 1990. The split polar vortex enhances meridional moisture transport from the Northern Atlantic

ZHANG ET AL. 8 of 12

and Pacific Oceans to the NKS (Figure S10a in Supporting Information S1). Meanwhile, the local anticyclonic anomalies reduce precipitation in the NKS (Figures 3a and 3c). Reduced cloud cover under these conditions amplifies surface solar radiation (Figure S10c in Supporting Information S1). Concurrently, the advected moisture (water vapor, an important greenhouse gas; Kapsch et al., 2013; Park et al., 2015; Zhou et al., 2024) combines with stronger solar radiation to increase surface temperatures (Figure S8a in Supporting Information S1), driving sea-ice melt. Thus, before 1990, positive dipole TPSC structure establishes a thermal regime conductive to negative NKS sea-ice anomalies (Figure 1b).

By comparison, post-1990, positive monopole TPSC-associated cyclonic anomalies strengthen the Arctic polar vortex, represented as a reduced vortex area and enhanced vortex intensity (Figure 4d). The correlations between the polar vortex area index and PC1\_TPSC are r = 0.08 (p > 0.1) before 1990 and r = -0.58 (p < 0.01) after 1990 (Figure S9b in Supporting Information S1), indicating monopole TPSC's dominance in modulating polar vortex area after 1990. This strengthened polar vortex suppresses meridional energy exchange. Reduced moisture transport and solar radiation (Figures S10b and S10d in Supporting Information S1) under these conditions depress temperatures in the BS region (Figure S8b in Supporting Information S1), favoring sea-ice growth. Collectively, these processes establish a thermal regime whereby the positive monopole TPSC pattern drives positive BS sea-ice anomalies (Figure 1d).

The TPSC-associated Arctic anticyclonic (pre-1990) and cyclonic (post-1990) anomalies generate corresponding wind stress patterns (Figures S11a and S11b in Supporting Information S1), which govern sea-ice dynamics through Ekman transport principles. In the Northern Hemisphere, oceanic surface circulation is deflected to the right of wind stress vectors. Prior to 1990, anticyclonic wind stress anomalies drive poleward Ekman drift of low-concentration sea-ice from the high-latitude Atlantic into the NKS (Figure S11c in Supporting Information S1), thereby reducing high-concentration sea-ice in the NKS. Conversely, post-1990, cyclonic wind stress anomalies induce equatorward Ekman drift of high-concentration sea-ice from Arctic center toward the North Atlantic sector, thereby increasing BS sea-ice concentration (Figure S11d in Supporting Information S1).

# 4. Summary and Discussions

Recent literature has disclosed the natural variability as a driver of Arctic sea-ice interannual variability, with factors such as ENSO (Luo et al., 2023), PNA (Liu et al., 2021), NAO, and Ural blocking (Luo et al., 2019). Our study advances this understanding by demonstrating that the transition in the TPSC pattern leads to a reversal in the spring TPSC-ice relationship.

The physical processes underlying these changes are summarized in Figures 4a and 4b. Shift in TPSC patterns influence local circulation and Rossby wave sources, leading to distinct circumglobal waviness. Before 1990, dipole TPSC-induced Arctic anticyclonic anomalies weaken the polar vortex, increasing NKS moisture intrusion and solar radiation, which raise temperatures and accelerate sea-ice melt. These anomalies also drive poleward sea-ice drift, transporting low-concentration ice to reduce NKS sea-ice concentration. After 1990, monopole TPSC-associated Arctic cyclonic anomalies strengthen the polar vortex, reducing BS moisture and solar radiation, cooling the atmosphere, and promoting sea-ice growth. These cyclonic anomalies enhance equatorward sea-ice drift, increasing BS ice concentration. Quantitative analysis further reveals that TPSC-driven contributions sea-ice anomalies account for 44.82% (NAOA) versus 39.10% (NSIDC) in the NKS region, and 35.01% (NAOA) versus 17.85% (NSIDC) in the BS sector (Figure 4e).

The monopole TPSC-associated circumglobal waviness exhibits longer propagation route with more atmospheric activity centers (Figures S7a and S7b in Supporting Information S1). This difference corresponds to latitudinal shift in turning position of the wave train: pre-1990, wave train deflects toward the Arctic via the North Pacific sector, whereas post-1990 trajectories redirect over the North America. Waveguide dynamics, quantified through potential vorticity gradient (PVG, Jia et al., 2019; Song et al., 2014), reveals that negative PVG anomalies (blue circle, Figures S7c and S7d in Supporting Information S1) spatially align with wave deflection zones. The weakened PVG post-1990 likely facilitate prolonged wave traveling through reduced Rossby wave reflection.

This study investigates the interannual linkage between TPSC and spring Arctic climate variability. Using the Linear Baroclinic Model, we show a 10-20-day teleconnection linking the TP and the Arctic (Figure S12 in Supporting Information S1), illustrating that Tibet-Arctic connection occurs not only on seasonal but also on subseasonal scales. Positive correlation emerges between western TPSC and Arctic sea-ice variability, suggesting

ZHANG ET AL. 9 of 12

Acknowledgments

University.

This work was supported by the National

Natural Science Foundation of China

Grants 42305016 (C.Z.) and 42030602

(A.D.). C.Z. acknowledges the funding

from the Chinese Scholarship Council

Outstanding Postdoctoral Scholarship,

(File No. 202306310194) and the

State Kev Laboratory of Marine

Environmental Science at Xiamen

that reduced snow cover may contribute sea ice reduction. Crucially, the post-1995 has witnessed accelerated snow cover decline in the western TP (Liu et al., 2024; Wu et al., 2012), implying a growing climatic influence on Arctic ice trends. Furthermore, preceding winter dipole/monopole-like TPSC patterns serve as the important precursors for spring sea ice anomalies (Figure S13 in Supporting Information S1). These findings have critical implications for enhancing the spring predictability barrier and improving future sea ice projections.

In the early 1990s, the interdecadal oscillation transitioned from negative to positive phase (e.g., Atlantic Multidecadal Oscillation, AMO; Day et al., 2012; Atlantic Multidecadal Variability, AMV; Chen et al., 2025) and from positive to negative phase (Interdecadal Pacific Oscillation, IPO; Wang et al., 2025). Crucially, the AMO's negative/positive phases and IPO's positive/negative exhibit spatial similarities with circulation patterns linked to dipole/monopole TPSC anomalies (Wang et al., 2025), whereas AMV's phase shift produces atmospheric responses opposite to AMO's in modulating TPSC-Arctic teleconnections (Chen et al., 2025). This suggests that the AMO/IPO likely plays a role in altering TPSC-ice relationship. Further investigation into these interdecadal modulation is crucial for a comprehensive understanding of changes in the Arctic sea-ice variability.

# **Data Availability Statement**

Data - The NSIDC weekly SCE are provided by Brodzik and Armstrong. (2013). Data for the NOAA weekly SCE are provided by Robinson et al. (2012). The HadISST sea-ice concentration data are provided by Rayner et al. (2003). The NSIDC sea-ice vector data are provided by Tschudi et al. (2019). The ORAS5 wind stress data are provided by Zuo et al. (2018). The ERA5 atmospheric data sets are provided by Hersbach et al. (2020). The GPCP precipitation data are provided by Adler et al. (2003). The CESM-LE experiment data sets are provided by C. Zhang (2025). Software - Data processing and figure plotting were conducted using the Grid Analysis and Display System (GrADS, v2.2.1) from Kinter and James (1994) and MATLAB v9.13.0. Model–Numerical simulations are performed using the CESM-LE version 1.2, as described in Kay et al. (2015).

#### References

Adler, R. F., Huffman, G. J., Chang, A., Ferraro, R., Xie, P.-P., Janowiak, J., et al. (2003). The Version-2 global precipitation climatology project (GPCP) monthly precipitation analysis (1979–Present) [Dataset]. *Journal of Hydrometeorology*, 4(6), 1147–1167. https://doi.org/10.1175/1525-7541(2003)004<1147:TVGPCP>2.0.CO:2

Brodzik, M. J., & Armstrong, R. (2013). Northern hemisphere EASE-grid 2.0 weekly snow cover and sea ice extent, version 4 (NSIDC-0046) [Dataset]. NASA National Snow and Ice Data Center Distributed Active Archive Center. https://doi.org/10.5067/P700HGJLYUQU

Bushuk, M., Winton, M., Bonan, D., Blanchard-Wrigglesworth, E., & Delworth, T. (2020). A mechanism for the arctic sea ice spring predictability barrier. *Geophysical Research Letters*, 47(13), e2020GL088335. https://doi.org/10.1029/2020GL088335

Chen, S., Chen, W., Wu, R., Yu, B., Graf, H. F., Cai, Q., et al. (2025). Atlantic multidecadal variability controls Arctic-ENSO connection. npj Climate and Atmospheric Science, 8(1), 44. https://doi.org/10.1038/s41612-025-00936-x

Climate and Atmospheric Science, 8(1), 44. https://doi.org/10.1038/841612-025-00936-x
Chen, S., Wu, R., Chen, W., & Yu, B. (2020). Influence of winter arctic sea ice concentration change on the El niño–southern oscillation in the

following winter. Climate Dynamics, 54(1–2), 741–757. https://doi.org/10.1007/s00382-019-05027-1
Chen, S. W., Chen, W., Zhou, R., Wu, R., Ding, S., Chen, L., et al. (2024). Interdecadal variation in the impact of arctic sea ice on El Niñosouthern oscillation: The role of atmospheric mean flow. Journal of Climate, 37(21), 5483–5506. https://doi.org/10.1175/JCLI-D-23-0733.1

Clancy, R., Bitz, C., & Blanchard-Wrigglesworth, E. (2021). The influence of ENSO on arctic sea ice in large ensembles and observations. Journal of Climate, 34, 1–50. https://doi.org/10.1175/ICLI-D-20-0958.1

Cohen, J., Agel, L., Barlow, M., Garfinkel, C., & White, I. (2021). Linking Arctic variability and change with extreme winter weather in the United States. Science, 373(6559), 1116–1121. https://doi.org/10.1126/science.abi9167

Dai, A., Luo, D., Song, M., & Liu, J. (2019). Arctic amplification is caused by sea-ice loss under increasing CO<sub>2</sub>. Nature Communications, 10(1), 121. https://doi.org/10.1038/s41467-018-07954-9

Day, J. J., Hargreaves, J. C., Annan, J. D., & Abe-Ouchi, A. (2012). Sources of multi-decadal variability in Arctic sea ice extent. *Environmental Research Letters*, 7(3), 034011. https://doi.org/10.1088/1748-9326/7/3/034011

Deng, J., & Dai, A. (2022). Sea ice-air interactions amplify multidecadal variability in the north Atlantic and arctic region. *Nature Communications*, 13(1), 2100. https://doi.org/10.1038/s41467-022-29810-7

Deng, J., & Dai, A. (2024). Arctic sea ice–air interactions weaken El Niño–southern oscillation. Science Advances, 10(13), eadk3990. https://doi.org/10.1126/sciadv.adk3990

org, 10.1120/schav.aux.3990

Ding, Q., Schweiger, A., L'Heureux, M., Battisti, D., Po-Chedley, S., Johnson, N., et al. (2017). Influence of high-latitude atmospheric circulation changes on summertime Arctic sea ice. *Nature Climate Change*, 7(4), 289–295. https://doi.org/10.1038/nclimate3241

Ding, Q., Schweiger, A., L'Heureux, M., Steig, E., Battisti, D., Johnson, N., et al. (2019). Fingerprints of internal drivers of Arctic sea ice loss in observations and model simulations. *Nature Geoscience*, 12(1), 28–33. https://doi.org/10.1038/s41561-018-0256-8

Ding, Q., Wallace, J. M., Battisti, D. S., Steig, E. J., Gallant, A. J. E., Kim, H.-J., & Geng, L. (2014). Tropical forcing of the recent rapid Arctic warming in northeastern Canada and Greenland. *Nature*, 509(7499), 209–212. https://doi.org/10.1038/nature13260

England, M. R., Polvani, L. M., Sun, L., & Deser, C. (2020). Tropical climate responses to projected Arctic and Antarctic sea-ice loss. *Nature Geoscience*, 13(4), 275–281. https://doi.org/10.1038/s41561-020-0546-9

Goodwell, A. E., Jiang, P., Ruddell, B. L., & Kumar, P. (2020). Debates—does information theory provide a new paradigm for Earth science? Causality, interaction, and feedback. *Water Resources Research*, 56(2), e2019WR024940. https://doi.org/10.1029/2019WR024940

ZHANG ET AL. 10 of 12

- Gottlieb, A. R., & Mankin, J. S. (2024). Evidence of human influence on northern hemisphere snow loss. *Nature*, 625(7994), 293–300. https://doi.org/10.1038/s41586-023-06794-y
- He, W., Chen, H., & Ma, J. (2023). Variations in summer extreme hot-humid events over eastern China and the possible associated mechanisms. Journal of Climate, 36(11), 3801–3815. https://doi.org/10.1175/JCLI-D-22-0695.1
- Hersbach, H., Bell, B., Berrisford, P., Hirahara, S., Horányi, A., Muñoz-Sabater, J., et al. (2020). The ERA5 global reanalysis [Dataset]. *Quarterly Journal of the Royal Meteorological Society*, 146(730), 1999–2049. https://doi.org/10.1002/qj.3803
- Immerzeel, W., Lutz, A., Andrade, M., Bahl, A., Biemans, H., Bolch, T., et al. (2020). Importance and vulnerability of the world's water towers. Nature, 577(7790), 364–369. https://doi.org/10.1038/s41586-019-1822-y
- Jia, X., You, Y., Wu, R., & Yang, Y. (2019). Interdecadal changes in the dominant modes of the interannual variation of spring precipitation over China in the Mid-1980s. *Journal of Geophysical Research: Atmospheres*, 124(20), 10676–10695. https://doi.org/10.1029/2019JD030901
- Johns, W. E., Baringer, M. O., Beal, L. M., Cunningham, S. A., Kanzow, T., Bryden, H. L., et al. (2011). Continuous, array-based estimates of Atlantic Ocean heat transport at 26.5°N. *Journal of Climate*, 24(10), 2429–2449. https://doi.org/10.1175/2010JCLI3997.1
- Kapsch, M. L., Graversen, R. G., & Tjernström, M. (2013). Springtime atmospheric energy transport and the control of Arctic summer sea-ice extent. Nature Climate Change, 3(8), 744–748. https://doi.org/10.1038/nclimate1884
- Kay, J. E., Deser, C., Phillips, A., Mai, A., Hannay, C., Strand, G., et al. (2015). The community earth system model (CESM) large ensemble project: A community resource for studying climate change in the presence of internal climate variability (model). Bulletin of the American Meteorological Society, 96(8), 1333–1349. https://doi.org/10.1175/BAMS-D-13-00255.1
- Kim, B. M., Son, S. W., Min, S. K., Jeong, J. H., Kim, S. J., Zhang, X., et al. (2014). Weakening of the stratospheric polar vortex by Arctic sea-ice loss. *Nature Communications*, 5(1), 4646. https://doi.org/10.1038/ncomms5646
- Kinter, J. L., & James, L. (1994). The grid analysis and display system (GrADS) (version 2.2.1) [Software]. Center for Ocean-land-AtmosphereStudies (COLA). https://ntrs.nasa.gov/citations/19950011076
- Kraaijenbrink, P., Stigter, E., Yao, T., & Immerzeel, W. W. (2021). Climate change decisive for Asia's snow meltwater supply. *Nature Climate Change*, 11, 1–7. https://doi.org/10.1038/s41558-021-01074-x
- Li, W., Guo, W., Qiu, B., Xue, Y., Hsu, P.-C., & Wei, J. (2018). Influence of Tibetan Plateau snow cover on East Asian atmospheric circulation at medium-range time scales. *Nature Communications*, 9(1), 4243. https://doi.org/10.1038/s41467-018-06762-5
- Liang, X. S. (2016). Information flow and causality as rigorous notions ab initio. *Physical Review E*, 94(5), 052201. https://doi.org/10.1103/PhysRevE.94.052201
- Liang, X. S., & Kleeman, R. (2005). Information transfer between dynamical system components. *Physical Review Letters*, 95(24), 244101. https://doi.org/10.1103/PhysRevLett.05.244101
- https://doi.org/10.1103/PhysRevLett.95.244101
  Liu, F., Jia, X., & Dong, W. (2024). Changes in spring snow cover over the eastern and Western Tibetan Plateau and their associated mechanism.
- Advances in Atmospheric Sciences, 41(5), 959–973. https://doi.org/10.1007/s00376-023-3111-9
  Liu, S., Wu, Q., Yao, Y., Schroeder, S., & Wang, L. (2022). Impacts of autumn-winter Tibetan Plateau snow anomalies on North Atlantic-Europe
- and Arctic climate. Journal of Geophysical Research: Atmospheres, 127(12). https://doi.org/10.1029/2021JD035791
- Liu, Z., Risi, C., Codron, F., He, X., Poulsen, C. J., Wei, Z., et al. (2021). Acceleration of western Arctic sea ice loss linked to the Pacific North American pattern. *Nature Communications*, 12(1), 1519. https://doi.org/10.1038/s41467-021-21830-z
- Luo, B., Luo, D., Ge, Y., Dai, A., Wang, L., Simmonds, I., et al. (2023). Origins of Barents-Kara sea-ice interannual variability modulated by the Atlantic pathway of El Niño-Southern Oscillation. *Nature Communications*, 14, 1–13. https://doi.org/10.1038/s41467-023-36136-5
- Luo, B., Luo, D., Wu, L., Zhong, L., & Simmonds, I. (2017). Atmospheric circulation patterns which promote winter arctic sea ice decline. Environmental Research Letters, 12(5), 1–13. https://doi.org/10.1088/1748-9326/aa69d0
- Luo, D., Chen, X., Overland, J., Simmonds, I., Wu, Y., & Zhang, P. (2019). Weakened potential vorticity barrier linked to recent winter Arctic sea ice loss and midlatitude cold extremes. *Journal of Climate*, 32(14), 4235–4261. https://doi.org/10.1175/JCLI-D-18-0449.1
- Mahajan, S., Zhang, R., & Delworth, T. L. (2011). Impact of the Atlantic meridional overturning circulation (AMOC) on Arctic surface air temperature and sea ice variability. *Journal of Climate*, 24(24), 6573–6581. https://doi.org/10.1175/2011JCL14002.1
- Neale, R. B., Richter, J., Park, S., Lauritzen, P. H., Vavrus, S. J., Rasch, P. J., & Zhang, M. (2013). The mean climate of the community atmosphere model (CAM4) in forced SST and fully coupled experiments. *Journal of Climate*, 26(14), 5150–5168. https://doi.org/10.1175/JCLI-D-12-00236.1
- Oleson, K., Lawrence, D., Bonan, G., Drewniak, B., Huang, M., Koven, C., et al. (2013). Technical description of version 4.5 of thecommunity land model (CLM). NCAR technical note NCAR/TN-503+STR. *National Center for Atmospheric Research*, 434.
- Park, H. S., Lee, S., Son, S. W., Feldstein, S. B., & Kosaka, Y. (2015). The impact of poleward moisture and sensible heat flux on Arctic winter sea ice variability. *Journal of Climate*, 28(13), 5030–5040. https://doi.org/10.1175/JCLI-D-15-0074.1
- Preece, J. R., Mote, T. L., Cohen, J., Wachowicz, L. J., Knox, J. A., Tedesco, M., & Kooperman, G. J. (2023). Summer atmospheric circulation over Greenland in response to Arctic amplification and diminished spring snow cover. *Nature Communications*, 14(1), 3759. https://doi.org/10.1038/s41467-023-39466-6
- Rayner, N. A., Parker, D., Horton, E. B., Folland, C., Alexander, L., Rowell, D., et al. (2003). Global analyses of sea surface temperature, sea ice, and night marine air temperature since the late nineteenth century [Dataset]. *Journal of Geophysical Research*, 108(D14). https://doi.org/10.1029/2002JD002670
- Robinson, D. A., Estilow, T. W., & Program, N. C. (2012). NOAA climate data record (CDR) of northern hemisphere (NH) snow cover extent (SCE), version 1 [NCDC: C00756] [Dataset]. NOAA National Centers for Environmental Information. https://doi.org/10.7289/V5N014G9
- Schweiger, A., Lindsay, R., Zhang, J., Steele, M., Stern, H., & Kwok, R. (2011). Uncertainty in modeled arctic sea ice volume. *Journal of Geophysical Research*, 116(C8), C00D06. https://doi.org/10.1029/2011JC007084
- Simmonds, I., & Li, M. (2021). Trends and variability in polar sea ice, global atmospheric circulations, and baroclinicity. *Annals of the New York Academy of Sciences*, 1504(1), 167–186. https://doi.org/10.1111/nyas.14673
- Smith, T., & Bookhagen, B. (2018). Changes in seasonal snow water equivalent distribution in high Mountain Asia (1987 to 2009). Science Advances, 4(1), e1701550. https://doi.org/10.1126/sciadv.1701550
- Song, J., Li, C., & Zhou, W. (2014). High and low latitude types of the downstream influences of the north Atlantic oscillation. *Climate Dynamics*, 42(3), 1097–1111. https://doi.org/10.1007/s00382-013-1844-3
- Stone, K., Solomon, S., & Kinnison, D. (2020). Prediction of northern hemisphere regional sea ice extent and snow depth using stratospheric ozone information. *Journal of Geophysical Research: Atmospheres*, 125(22). https://doi.org/10.1029/2019JD031770
- Sumata, H., de Steur, L., Divine, D., Granskog, M., & Gerland, S. (2023). Regime shift in Arctic Ocean sea ice thickness. *Nature*, 615(7952), 443–449. https://doi.org/10.1038/s41586-022-05686-x

ZHANG ET AL. 11 of 12

- Tang, S., Piao, S., Holland, D. M., Kan, F., Wang, T., Yao, T., & Li, X. (2024). Resonance between projected Tibetan Plateau surface darkening and Arctic climate change. Science Bulletin, 69(3), 367–374. https://doi.org/10.1016/j.scib.2023.12.008
- Thackeray, C. W., & Hall, A. (2019). An emergent constraint on future Arctic sea-ice albedo feedback. *Nature Climate Change*, 9(12), 972–978. https://doi.org/10.1038/s41558-019-0619-1
- Topál, D., Ding, Q., Ballinger, T. J., Hanna, E., Fettweis, X., Li, Z., & Pieczka, I. (2022). Discrepancies between observations and climate models of large-scale wind-driven Greenland melt influence sea-level rise projections. *Nature Communications*, 13(1), 6833. https://doi.org/10.1038/ s41467-022-34414-2
- Tschudi, M., Meier, W. N., Stewart, J. S., Fowler, C., & J, M. (2019). Polar pathfinder daily 25 km EASE-grid sea ice motion vectors, version 4 (NSIDC-0116) [Dataset]. NASA National Snow and Ice Data Center Distributed Active Archive Center. https://doi.org/10.5067/O57VAIT2AYYY
- Wang, C., Yang, K., Li, Y., Wu, D., & Bo, Y. (2017). Impacts of spatiotemporal anomalies of Tibetan Plateau snow cover on summer precipitation in eastern China. *Journal of Climate*, 30(3), 885–903. https://doi.org/10.1175/JCLI-D-16-0041.1
- Wang, L., Chen, S., Chen, W., Wu, R., & Wang, J. (2025). Interdecadal variation of springtime compound temperature-precipitation extreme events in China and its association with Atlantic multidecadal oscillation and interdecadal Pacific oscillation. *Journal of Geophysical Research:* Atmospheres, 130(2), e2024JD042503. https://doi.org/10.1029/2024JD042503
- Wu, Z., Jiang, Z., Li, J., Zhong, S., & Wang, L. (2012). Possible association of the Western Tibetan Plateau snow cover with the decadal to interdecadal variations of northern China heatwave frequency. Climate Dynamics, 39(9–10), 2393–2402. https://doi.org/10.1007/s00382-012-1439-4
- Xiao, Z., & Duan, A. (2016). Impacts of Tibetan Plateau snow cover on the interannual variability of the East Asian summer monsoon. *Journal of Climate*, 29(23), 8495–8514. https://doi.org/10.1175/JCLI-D-16-0029.1
- Xie, Y., Duan, A., Zhang, C., He, C., Mao, Q., & Liu, B. (2025). Reversed link between central Pacific ENSO and greenland–barents sea ice. npj Climate and Atmospheric Science, 8(1), 28. https://doi.org/10.1038/s41612-025-00912-5
- Xu, X., Lu, C., Shi, X., & Gao, S. (2008). World water tower: An atmospheric perspective. Geophysical Research Letters, 35(20). https://doi.org/10.1029/2008GL035867
- Xu, X., Sun, C., Chen, D., Zhao, T., Xu, J., Zhang, S., et al. (2021). A vertical transport window of water vapor in the troposphere over the Tibetan Plateau with implications for global climate change. *Atmospheric Chemistry and Physics*, 22(2), 1149–1157. https://doi.org/10.5194/acp-22-1149-2022
- Yasunari, T., Kitoh, A., & Tokioka, T. (1991). Local and remote responses to excessive snow mass over eurasia appearing in the northern spring and summer climate: A study with the MRI-GCM. *Journal of the Meteorological Society of Japan. Ser. II*, 69(4), 473–487. https://doi.org/10.2151/jmsi1965.69.4 473
- Yi, B., & Bose, S. (2022). Quantum liang information flow as causation quantifier. *Physical Review Letters*, 129(2), 020501. https://doi.org/10.1103/PhysRevLett.129.020501
- Zhang, C. (2025). Tibetan Plateau snow experiments [Dataset]. Zenodo. https://doi.org/10.5281/zenodo.15058045
- Zhang, C., Duan, A., Jia, X., Hu, J., & Liu, S. (2023). Snow cover on the Tibetan Plateau and Lake Baikal intensifies the winter north Atlantic oscillation. Geophysical Research Letters, 50(16), e2023GL104754. https://doi.org/10.1029/2023GL104754
- Zhang, C., Duan, A., Jia, X., Wang, Z., & Pan, Z. (2023). A dynamic link between spring arctic sea ice and the Tibetan Plateau snow increment indicator. npj Climate and Atmospheric Science, 6(1), 191. https://doi.org/10.1038/s41612-023-00505-0
- Zhang, C., Guo, Y., & Wen, Z. (2022). Interdecadal change in the effect of Tibetan Plateau snow cover on spring precipitation over eastern China around the early 1990s. Climate Dynamics, 58(9), 2807–2824. https://doi.org/10.1007/s00382-021-06035-w
- Zhang, C., & Jia, X. (2022). The seasonal evolution of the Tibetan Plateau snow cover related moisture during spring-to-summer. *Journal of Geophysical Research: Atmospheres*, 127(11), e2022JD036560. https://doi.org/10.1029/2022JD036560
- Zhang, C., Jia, X., Duan, A., & Hu, D. (2023). Interdecadal changes in the dominant modes of spring snow cover over the Tibetan Plateau around the early 1990s. *Journal of Climate*, 36(11), 3765–3780. https://doi.org/10.1175/JCLI-D-22-0487.1
- Zhang, C., Jia, X., & Wen, Z. (2021). Increased impact of the Tibetan Plateau spring snow cover to the Mei-yu rainfall over the Yangtze river valley after the 1990s. *Journal of Climate*, 34(14), 5985–5997. https://doi.org/10.1175/jcli-d-21-0009.1
- Zhang, P., Chen, G., Ting, M., Ruby Leung, L., Guan, B., & Li, L. (2023). More frequent atmospheric Rivers slow the seasonal recovery of Arctic sea ice. Nature Climate Change, 13(3), 266–273. https://doi.org/10.1038/s41558-023-01599-3
- Zhang, T., Wang, T., Krinner, G., Wang, X., Gasser, T., Peng, S., et al. (2019). The weakening relationship between Eurasian spring snow cover and Indian summer monsoon rainfall. *Science Advances*, 5(3), eaau8932. https://doi.org/10.1126/sciadv.aau8932
- Zhou, B., Song, Z., Yin, Z., Xu, X., Sun, B., Hsu, P., & Chen, H. (2024). Recent autumn sea ice loss in the eastern arctic enhanced by summer Asian-Pacific oscillation. *Nature Communications*, 15(1), 2798. https://doi.org/10.1038/s41467-024-47051-8
- Zuo, H., Balmaseda, M. A., Mogensen, K., & Tietsche, S. (2018). OCEAN5: The ECMWF ocean reanalysis system and its real-time analysis component [Dataset]. ECMWF Technical Memoranda. https://doi.org/10.21957/la2v0442

# **References From the Supporting Information**

- Chen, Y., Duan, A., & Li, D. (2021). Connection between winter arctic sea ice and west Tibetan Plateau snow depth through the NAO. *International Journal of Climatology*, 41(2), 846–861. (Supporting Information). https://doi.org/10.1002/joc.6676
- Hoskins, J. I., & White, G. (1983). The shape, propagation and mean-flow interaction of large-scale weather systems. *Journal of the Atmospheric Sciences*, 40(Supporting Information), 1595–1612. https://doi.org/10.1175/1520-0469(1983)040<1595:TSPAMF>2.0.CO;2
- Huang, J., Zhou, X., Wu, G., Xu, X., Zhao, Q., Liu, Y., et al. (2023). Global climate impacts of land-surface and atmospheric processes over the Tibetan Plateau. Reviews of Geophysics, 61(3), e2022RG000771. https://doi.org/10.1029/2022RG000771
- Li, F., Wan, X., Wang, H., Orsolini, Y. J., Cong, Z., Gao, Y., & Kang, S. (2020). Arctic sea-ice loss intensifies aerosol transport to the Tibetan Plateau. *Nature Climate Change*, 10(11), 1037–1044. (Supporting Information). https://doi.org/10.1038/s41558-020-0881-2
- Watanabe, M., & Kimoto, M. (2000). Atmosphere-ocean thermal coupling inthe north Atlantic: A positive feedback. *Quarterly Journal Of The Royal Meteorological Society*, 126(570), 3343–3369. (Supporting Information). https://doi.org/10.1002/qi.49712657017
- Yanai, M., Esbensen, S., & Chu, J.-H. (1973). Determination of bulk properties of tropical cloud clusters from large-scale heat and moisture budgets. *Journal of the Atmospheric Sciences*, 30(4), 611–627. (Supporting Information). https://doi.org/10.1175/1520-0469(1973)030<0611: DOBPOT>2.0.CO:2

ZHANG ET AL. 12 of 12